

# Experimental search for anisotropic flux flow resistivity in the $a$ - $b$ plane of optimally doped epitaxial thin films of $YBa_2Cu_3O_{7-\delta}$

G. Koren, P. Aronov and E. Polturak

*Department of Physics, Technion - Israel Institute of Technology, Haifa 32000, Israel\**

(Dated: November 13, 2018)

Transport measurements along the node and anti-node directions in the  $a$ - $b$  plane of optimally doped and epitaxial thin films of  $YBa_2Cu_3O_{7-\delta}$  are reported. Low bias magnetoresistance measurements near and below  $T_c$  show that the flux flow resistivity along the node and anti-node directions versus magnetic field are indistinguishable. This result suggests that within the experimental error of our measurements, *no* correspondence is found between the flux pinning properties in YBCO and the d-wave nature of the order parameter.

Under applied magnetic field, the apparent resistance of type II superconductors in the mixed state is due to the motion of vortices. In the presence of transport current, the Lorentz (or Magnus) force on vortices causes motion and induces a voltage drop across the superconducting sample. The ratio of the induced voltage divided by the current defines the flux flow resistance [1, 2]. In the Bardeen-Stephen model [3], valid for the case of weak pinning as for instance near  $T_c$ , the effective viscosity associated with the motion of vortices is caused by the interaction of the transport current and the shielding currents around the vortex. In the cuprates, the shielding currents around the vortex are predicted to show anisotropy linked to the d-wave nature of the order parameter [4, 5]. Under the quasiclassical approximation and by the use of the Eilenberger equations, Ichioka *et al* found a small four fold anisotropy of a few percents in the induced supercurrents around the vortex core [4]. A preliminary microscopic calculation of vortex tunneling also seems to yield an *anisotropic* vortex dynamics [5]. It is therefore plausible to assume that the effective viscosity which determines the flux flow resistivity may also be anisotropic. The search for this effect is the subject of the present study. We designed a specific, high precision experiment to look for it by Magnetotransport measurements which were conducted on nominally identical thin film microbridges of YBCO patterned on the same wafer along the node and antinode directions of the d-wave order parameter. We found that the flux flow resistance at low bias did not reveal any anisotropy at the 1% level, which is the stated precision of our measurements.

To facilitate the comparison between the transport properties along the node and antinode directions, two high quality  $c$ -axis oriented epitaxial thin films of YBCO were prepared under identical conditions by laser ablation deposition on (100)  $SrTiO_3$  (STO) wafers of  $10 \times 10 \text{ mm}^2$  area. In one case, the orientation of the single crystal STO substrate was with the edge of the wafer parallel to the (010) crystalline direction, while in the other case it was parallel to the (110) direction. Ten

microbridges were defined on each wafer using the same photolithographic mask, and patterned by Ar ion milling at a temperature of  $-170 \text{ }^\circ\text{C}$ . The dimensions of the microbridges were  $0.12 \times 12 \times 100 \text{ }\mu\text{m}^3$ . Successive microbridges were oriented at alternating angles of  $0^\circ$  and  $45^\circ$  to the edge of the wafers, so that the transport current would flow either along the node or the antinode of the order parameter. The alternating direction of *adjacent* microbridges was important to minimize systematic differences due to possible inhomogeneities in the films. On the first wafer with the side parallel to the (010) orientation, five odd number bridges were along the antinode direction, and five even number bridges along the node direction. In the second wafer with the side parallel to the (110) orientation, the role of the antinode and node bridges was reversed due to the epitaxial growth of the film. Studying these two types of wafers was done in order to check if our ion milling process, done at an incident angle of  $45^\circ$  to the wafers, is affecting the properties of the microbridges. We note that on the first wafer, the Ar ions milling process leads to antinode bridges with sides normal to the surface, but at an oblique angle for the node microbridges. This situation is reversed in the second wafer. Any observed difference in the transport properties of the two wafers would imply that the effect is not intrinsic, and results from the patterning process. Low resistance gold contacts were prepared on the two wafers by laser ablation deposition and lift off, followed by further oxygen annealing for the gold/YBCO contact (at  $650^\circ\text{C}$ ) and the YBCO films themselves (at  $450^\circ\text{C}$ ). Transport measurements were done by the standard 4-probe dc technique, with and without a magnetic field of up to 8T normal to the wafers (parallel to the  $c$ -axis).

Figures 1 and 2 show mean values of the zero field normal state resistivity  $\rho$  and critical current density  $J_c$  on the two wafers, as a function of temperature. The mean values were obtained for each wafer by averaging over three microbridges of each type (node or antinode) which had the closest  $T_c$ (R=0) values. The critical current data was measured using a  $1 \text{ }\mu\text{V}$  per  $100 \text{ }\mu\text{m}$  bridge length criterion. The normal state resistivities along the

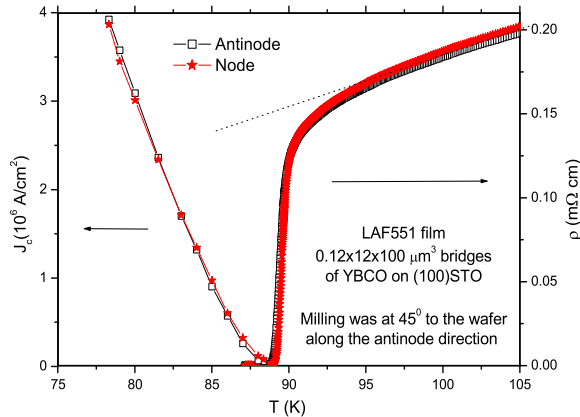


FIG. 1: (Color on-line) Mean resistivity and critical current density versus temperature of three microbridges of YBCO along an anti-node direction (squares), and three along a node direction (stars). The antinode bridges are parallel to the (100) side of the STO wafer, and the node bridges are oriented at  $45^\circ$  to it. The lines connecting the data points are guide to the eye. The straight dashed line extrapolating the normal state resistivity to lower temperatures shows that  $T_c(\text{onset})$  is  $\sim 94\text{K}$ .

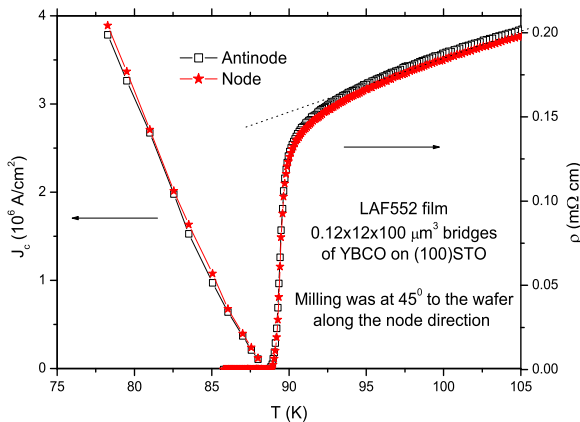


FIG. 2: (Color on-line) Mean resistivity and critical current density versus temperature of three microbridges of YBCO along an anti-node direction (squares), and three along a node direction (stars). The node bridges are parallel to the (110) side of the STO wafer, and the node bridges are oriented at  $45^\circ$  to it. The lines connecting the data points are guide to the eye.

node and antinode directions are slightly different, by about 2%. In Fig. 1 the node resistivity is higher, and in Fig. 2 the opposite situation is found where the antinode resistivity is higher. This behavior results from the fact that the ion milling process slightly damages the side of the bridges which are exposed to the Ar ion beam,

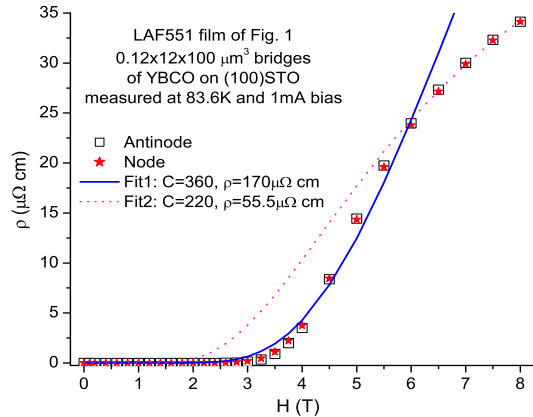


FIG. 3: (Color on-line) Mean flux flow resistivity at 83.6K versus applied magnetic field of the bridges of Fig. 1. The mean values are of three bridges along the node direction (stars), and three along the anti-node direction (squares). The two curves are fits using the Tinkham's model as given by Eq. (1).

the node bridges in Fig. 1 and the antinode bridges of Fig. 2. Apart from this minor difference,  $\rho(\text{node})$  should be equal to  $\rho(\text{anti-node})$  since our films are heavily twinned. This results from the fact that due to twinning one has  $\rho = (\rho_a + \rho_b)/2$  for the anti-node bridges, and  $\rho = \rho_a \cos^2(45^\circ) + \rho_b \sin^2(45^\circ)$  for the node bridges, which are of course equal. The transition temperatures  $T_c(\text{onset})$  in Figs. 1 and 2 are identical for both type of bridges.  $T_c(\text{onset}) \sim 94\text{K}$  is the temperature at which the resistivity data in Figs. 1 and 2 deviates from the straight dashed line extrapolating the high temperature data to lower temperatures. The transition temperatures of zero resistance  $T_c(R=0)$  of the node and antinode bridges are very close. In Fig. 1 the values are 88.9K for the antinode bridges and 89.1K for the node ones, while in Fig. 2 the corresponding values are 88.8K and 88.9K. Although within the experimental noise, the slightly higher  $T_c$  by about 0.1% of the node microbridges as compared to the antinode ones, is consistent with Ichioka *et al.* results where the supercurrent around a vortex is slightly higher along the node directions [4]. The differences between the node and anti-node bridges are also very small in the critical current results, where near  $T_c$  the small difference in  $T_c$  affects the results, but at lower temperatures this difference is within the experimental noise. For temperatures close to  $T_c(R=0)$ ,  $J_c(T)$  increases with decreasing temperature as  $(T_c - T)^{3/2}$ , and linearly at lower temperatures with a slope of  $0.45 \times 10^6 \text{ A/cm}^2\text{K}$ . So we can conclude from Figs. 1 and 2 that the node and antinode bridges have almost identical  $T_c$  and  $J_c(T)$ .

Fig. 3 and Fig. 4 show the flux flow resistivity of

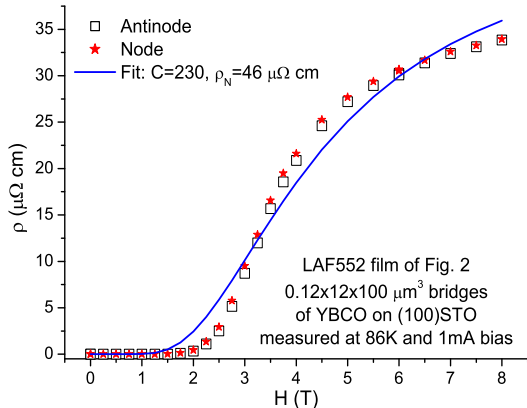


FIG. 4: (Color on-line) Mean flux flow resistivity at 86K versus applied magnetic field of the bridges of Fig. 2. The mean values are of two bridges along the node direction (stars), and two along the anti-node direction (squares). Mean values were taken here over two and not three microbridges due to contact problems with one of the bridges. The curve is a fit using the Tinkham's model as given by Eq. (1).

microbridges of Fig. 1 and Fig. 2, respectively, as a function of applied magnetic field normal to the wafers. The onset field at which the flux flow resistivity first appears increases with decreasing temperature, due to the stronger pinning of vortices at lower temperatures. Figs. 3 and 4 show that the flux flow resistivity curves versus field of both kinds of microbridges, those along the node and anti-node directions are almost indistinguishable. This is the main experimental observation of the present study. Both figures also show that at high fields the flux flow resistivity tends to saturate, more so in Fig. 4 than in Fig. 3 due to the higher temperature. This is possibly due to a cross over to the normal state resistivity, although the measured value just above the transition  $\rho_N(95K) = 170 \mu\Omega cm$  (see Figs. 1 and 2) is much higher than the  $40 - 50 \mu\Omega cm$  value which can be extrapolated from Figs. 3 and 4. The overall behavior of  $\rho$  versus  $H$  is consistent with previous experiments on YBCO [6, 7]. From the linear part of the data with the highest slope, one can extract the critical field  $H_{c2}$  by using the Bardeen-Stephen model [2, 3, 6, 7]. The curves in Figs. 3 and 4 are two Ambegaokar-Halperin type fits using Tinkham's model [8, 9] which yields:

$$\rho_{ff} = \rho_N [I_0(U_0/2k_B T)]^{-2} = \rho_N [I_0(C(1-t)^{3/2}/H)]^{-2} \quad (1)$$

where  $\rho_{ff}$  and  $\rho_N$  are the flux flow and normal state resistivities,  $I_0$  is the modified Bessel function,  $U_0$  is the activation energy,  $t = T/T_c$  is the reduced temperature, and  $C$  is a constant. The basic physics behind this model is that the motion of vortices between pinning sites is thermally activated and involves phase slippage of  $2\pi$

like in a single heavily damped current driven Josephson junction. One sees that the fits can not reproduce the main features of the data all at once. In Fig. 3, we chose to show that they can either fit the data reasonably well up to a field of 6T but miss the higher fields data (solid curve), or fit the higher fields but miss the onset and the intermediate fields data (dashed curve). In Fig. 4 we chose to show a single fit for the whole range of fields, but than the fit quality is quite poor. We note that the low fields fit in Fig. 3 (Fit1) is obtained with the actually measured normal state resistivity just above  $T_c(\text{onset})$  at 95K ( $170 \mu\Omega cm$ ). We shall discuss the reliability and suitability of the Tinkham model later on, here we point out that the important thing is that the model allows us to obtain the activation energy  $U_0$  which is related to the fit parameter  $C$  by  $U_0 = 2k_B T_c t(1-t)^{3/2} C/H$  as seen in Eq. (1). Since the node and antinode curves in Figs. 3 and 4, respectively are almost identical, the same  $U_0$  is obtained for both orientations for each temperature. Therefore, at any given temperature, the activation energy for moving vortices along both directions is the same. This is the main result of the present study. It indicates that the pinning properties of YBCO which control the flux flow resistivity are fully isotropic to within the experimental error, and are not affected by the intrinsic anisotropy of the d-wave order parameter as might be expected.

Finally, we discuss the suitability of using the Tinkham model given by Eq. (1) for the present results. We have already seen the problems involved in using this model in the fits of Figs. 3 and 4. To elucidate this issue, we show in Fig. 5 the flux flow resistivity data versus magnetic field of a microbridge on LAF552 with a weak link in it (a scratch). The weak link leads to a very small critical current in this bridge, and the onset of the flux flow resistivity occurs at a very small field. The solid curve is a fit of this data using Eq. (1). One can see that in this bridge the Tinkham model of vortex motion by thermal activation fits the data quite nicely except for fields below about 1.5T. In this regime a different mechanism must be involved in the resistivity behavior versus field and we propose tunneling of vortices as a plausible explanation for the observed result. The standard tunneling probability for crossing a potential barrier of height  $V$  and width  $d$  is proportional to  $\exp[-k\sqrt{V}d]$  where  $k$  is a constant. In the present case, the barrier height is given by the activation energy of the vortex  $U_0$ , and the barrier width by the distance between adjacent pinning centers. We take an Anderson-Kim type activation energy given by Yeshurun and Malozemoff  $U_0 \propto 1/H$  (see Eq. (1)) [8, 10], and assume a constant tunneling distance between adjacent pinning centers in the weak link as this depends on the specific material properties and not on the magnetic field. This yields a flux flow tunneling current which is proportional to the flux flow resistivity, that

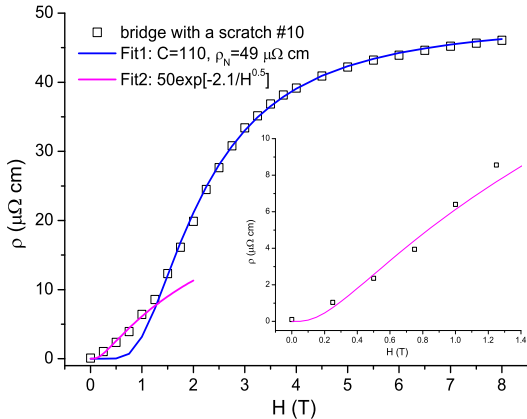


FIG. 5: (Color on-line) Main panel: Flux flow resistivity of an antinode bridge with a weak link (a scratch) on LAF552 versus applied magnetic field. The curves are fits to the experimental data. Fit1 is obtained by using the Tinkham's model of Eq. (1), and Fit2 is achieved by the tunneling model of Eq. (2). Inset: zoom up on the low field regime with the tunneling model fit.

for any given temperature is given by:

$$\rho_t = A \exp[-D/\sqrt{H}] \quad (2)$$

where  $A$  and  $D$  are constants. A fit of the data in Fig. 5 up to 2T using Eq. (2) is shown in this figure and its inset. A reasonably good fit is now obtained for the low fields regime, with a cross over to the Tinkham's model at higher fields. It therefore seems that the Tinkham model is appropriate for films with weak links or defects but not in the low fields regime. For instance, we could fit the data of Kunchur *et al.* [7] who used films with many defects and weak links reasonably well, but again, not in the low field regime where vortex tunneling apparently takes place (similarly to the corresponding fit in Fig. 5). Also, the original Ambegaokar and Halperin model [9] which was used by Tinkham in his model, was derived for a Josephson junction or a weak link. It is thus not surprising that better fits are obtained when weak links

are involved.

In conclusion, at temperatures close to  $T_c$ , low bias and within the experimental error of our measurements, a clear flux flow resistivity isotropy was observed in the present study for the node and anti-node directions in the  $a$ - $b$  plane of thin YBCO films. It is therefore demonstrated that the anisotropic d-wave nature of the order parameter in YBCO does not induce any measurable anisotropy in the flux pinning properties of the films. We also show that the Ambegaokar and Halperin type model used by Tinkham is more successful in films with weak links.

We are grateful to Rudolf P. Huebener, Guy Deutscher, Assa Auerbach and Lior Shkedy for useful discussions. This research was supported in part by the Israel Science Foundation (grant No. 1565/04), the Heinrich Hertz Minerva Center for HTSC, the Karl Stoll Chair in advanced materials, and the Fund for the Promotion of Research at the Technion.

---

\* Electronic address: gkoren@physics.technion.ac.il;  
URL: <http://physics.technion.ac.il/~gkoren>

- [1] R. P. Huebener, *Magnetic Flux Structures in Superconductors*, (Springer Verlag, 2nd edition, 2001).
- [2] M. Tinkham, *Introduction to Superconductivity*(McGraw-Hill, 2nd edition, 1996).
- [3] J. Bardeen and M.J. Stephen, Phys. Rev. **140**, A1197 (1965).
- [4] M. Ichioka, N. Hayashi, N Enomoto and K. Machida, Phys. Rev. B **53**, 15316 (1996).
- [5] Ari Mizel, cond-mat 0107530, (2001).
- [6] J.G. Ossandon *et al.*, Phys. Rev. B **45**21, 12534 (1992).
- [7] M.N. Kunchur, D.K. Christen and J.M. Phillips, Phys. Rev. Lett. **70**, 998 (1993).
- [8] M. Tinkham, Phys. Rev. Lett. **61**, 1658 (1988).
- [9] V. Ambegaokar and B. I. Halperin, Phys. Rev. Lett. **22**, 1364 (1969).
- [10] Y. Yeshurun and A. P. Malozemoff, Phys. Rev. Lett. **60**, 2202 (1988).